

THE STRUCTURAL CHARACTERIZATION, INVESTIGATION VIA THERMOLUMINESCENCE AND RADIOLUMINESCENCE PROPERTIES OF SAROS GULF CLAY SAMPLE

İlker Çetin KESKİN¹

Accepted: 2023-12-24
DOI: 10.47118/somatbd.1403544

ABSTRACT

Clay is mainly composed of illite, kaolinite, montmorillonite groups. Although it is abundant in nature, it is very difficult to find pure clay. The substances that make up clay are hydrous aluminum silicates. Each clay group contains different metal oxides or organic compounds. These impurities contained in minerals constitute an interesting field in luminescence and optical studies.

Although there are many studies on clay minerals, each sample shows its own unique characteristics. In this study, clay samples taken from Edirne-Keşan-Erikli Beach, located on the coast of Saros Gulf, were studied. Its crystallographic structure was determined by XRD analysis, its rheological properties and the elements it contained were determined by SEM-EDX analysis, and its structural properties were examined by FT-IR analysis. In optical absorption analysis, strong absorption bands were observed in the UV and Vis regions. In radioluminescence (RL) analysis, the emission spectrum formed by X-ray excitation are discussed. Likewise, in the thermoluminescence (TL) analysis using X-ray as primary excitation, peaks were observed in shallow and deep traps.

Keywords: Minerals, Clay, Impurities, Radioluminescence, Thermoluminescence

SAROS KÖRFEZİ KİL ÖRNEĞİNİN YAPISAL KARAKTERİZASYONU, TERMOLUMİNESANS VE RADYOLÜMİNESANS ÖZELLİKLERİNİN İNCELENMESİ

ÖZET

Kil, temel olarak illit, kaolinit, montmorillonit grupları olarak adlandırılmaktadır. Doğada bol miktarda bulunmakla birlikte saf kil bulmak oldukça zordur. Kili meydana getiren maddeler sulu alüminyum silikatlardır. Her kil grubu içerisinde farklı metal oksitler veya organik bileşikler barındırmaktadır. Minerallerin barındırdığı bu safsızlıklar lüminesans ve optik çalışmalarında ilgi çekici bir alan oluşturmaktadır.

Kil mineralleri üzerine pek çok çalışma bulunmakla birlikte herbir örnek kendine özgü özellikler göstermektedir. Bu çalışmada Saros Körfezine kıyısı bulunan Edirne-Keşan-Erikli Sahilinden alınan kil örnekleri ile çalışılmıştır. XRD analizi ile kristalografik yapısı belirlenmiş, reolojik özellikleri ve içerdiği elementler SEM-EDX analizi ile tespit edilmiş, FT-IR analizi ile

¹ Doç. Dr., Manisa Celal Bayar Üniversitesi Soma Meslek Yüksekokulu, Elektrik ve Enerji Bölümü, Manisa, ilker.keskin@cbu.edu.tr

yapısal özellikleri incelenmiştir. Optik absorpsiyon analizinde UV ve Vis bölgede güçlü soğurma bandları gözlenmiştir. Radyolüminesans (RL) analizinde X ışını uyarımı ile oluşan ışımada bandları tartışılmıştır. Yine birincil uyarım olarak X ışını kullanılarak alınan termolüminesans (TL) analizinde sıg ve derin tuzaklara pikler görülmüştür.

Optik absorpsiyon analizinde UV bölgede ve 273, 330, 465, 510 nm'de güçlü soğurma bandları gözlenmiştir. RL analizinde yaklaşık 550, 610, 720 ve 850 nm'de geniş emisyonlar gözlenmiştir. Alınan ölçümlerde 250 °C'deki ana pikin yanı sıra yaklaşık 100 ve 340 °C civarında TL pikleri görülmüştür.

Anahtar Kelimeler: Mineraller, Kil, Safsızlıklar, Radyolüminesans, Termolüminesans

1. INTRODUCTION

Natural clay is mainly composed of illite ($K_{0.65}Al_2(Al_{0.65}Si_{3.35}O_{10})(OH)_1$), kaolinite ($Al_2O_3 \cdot 2SiO_2 \cdot 2H_2O$), montmorillonite ($(Na, Ca)_{0.33}(Al, Mg)_2(Si_4O_{10})(OH)_2 \cdot nH_2O$). Fine-grained natural soil material containing clay minerals is encompassed by the term "clay." Plasticity emerges in clays when exposed to moisture, yet the potential for hardening is latent through firing processes. A pervasive substance, clay finds itself in the composition of shale, the most prevalent sedimentary rock primarily constituted by clay[1]. While natural deposits frequently feature a combination of silts and clay, distinctions between clays and other fine-grained soils manifest in variations of size and mineralogical composition.[2]

The high surface area of clay minerals is conferred by the diminutive size and plate-like structure of clay particles. In certain clay minerals, a negative electrical charge is carried by the plates, and this charge is counterbalanced by a surrounding layer of positive ions (cations), such as Na, K, or Ca. When the clay is combined with a solution containing alternative cations, an exchange can occur wherein these ions replace the existing cations in the layer surrounding the clay particles. This imparts to clays a substantial capacity for ion exchange.[3]

Many natural minerals used in radiation studies exhibit thermoluminescent (TL) properties, which depend on their formations, chemical compositions, impurity contents, and geological histories. Some natural minerals and synthetic crystals may possess effective dosimetric TL characteristics. Numerous studies focus on exploring the potential use of these minerals for dosimetric purposes or understanding trap structures and defects within minerals. Among these mineral groups, natural clay is a significant member of hydrous aluminum silicates family.[4, 5] In the past few decades, research on radiation-induced defects in minerals has gained significance. Thermoluminescence (TL) is a valuable technique employed to understand mechanisms of trapped electron capture and release resulting from the interaction of radiation with existing defects in the material lattice.[6, 7]

Cage, impurity, and structural defects, and their distributions in insulating minerals affect luminescent emission commonly observed when stimulated through various means such as X-rays, ions, electrons, temperature, or light. Therefore, radioluminescence is deemed an appropriate system for material characterization.[8, 9]

The radioluminescence (RL) technique involves the conversion of high-energy ionizing radiation, such as photons, by radioluminescent or scintillator materials into numerous visible-ultraviolet low-energy photons almost instantaneously. Within the RL phenomenon, the host material, initially excited by high-energy radiation, facilitates the migration of absorbed energy to the rare earth (RE) emission center, leading to the emission of photons through a relaxation process. Scintillator materials find applications in various fields, including nuclear physics detectors, medical imaging technologies (for the detection of high-energy photons and

accelerated particles), as well as high-energy and sophisticated industrial applications.[10, 11] RL system provides detailed spectral data through volumetric stimulation of the sample, although the setup and data collection process can be challenging. The RL system allows for the stimulation of the entire volume of the material with high-energy X-rays, enabling the detailed determination of emission spectra, especially for minerals with different impurity atoms.[12]

In this study, the structure of natural clay was characterized and its optical behavior was examined. On the other hand, the relationship between the emissions obtained after exposure to X-rays and the metal ions in the sample was investigated. In addition, the TL behavior of the clay sample irradiated with X-ray for different times was observed.

2. EXPERIMENTAL DETAILS

The X-ray diffraction (XRD) pattern and phase analysis of natural clay were conducted using a PANanalytical Empyrean X-ray diffraction device at room temperature. The clay's XRD pattern was compared to the standard ICSD. XRD patterns were recorded within the interval of 10° - 80° (2θ) at a speed of $0.0445^{\circ}/s$. The X-ray tube of this device was set to operate at a rated voltage of 10-60 kV, a rated current of 8-60 mA, and a maximum rated output phase control of 6 kW, with the slit size in the X-ray generator established as 0.4785° . Cu-K α (1.5405 \AA) was used as the radiation source. The FTIR spectra were recorded for absorbance in the region 400 – 4000 cm^{-1} using an Agilent Technologies Cary 660 Spectrometer. Scanning electron microscopy (SEM-EDS) images were used to examine the morphology of clay by using a Gemini SEM500. Optical absorption spectra of the clay sample were recorded in the wavelength region of 200 – 2000 nm using Perkin-Elmer Lambda 950 spectrophotometer.



Figure 1. Collecting location of the clay samples

While the RL emission spectrum of the clay powder, excitation was made with a Machlett OEG-50A X-ray tube operated at level of 30 kV and 15 mA. The detection of RL emission was

carried out using a Yobin Yvon spectrometer, which was coupled to a CCD detector cooled with liquid nitrogen. The irradiated samples for TL analysis were examined in a dark room using a RA94 Reader/Analyzer system, employing a linear heating rate of 2 °C/s, ranging from 50 °C up to 400 °C in a nitrogen (N₂) atmosphere.

3. RESULTS AND DISCUSSION

3.1 XRD Analysis

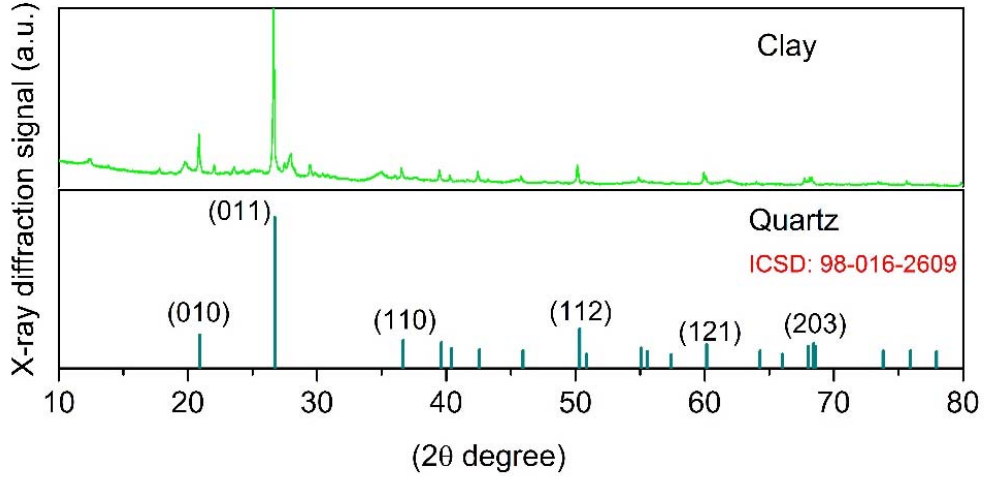


Figure 2. X-ray diffraction (XRD) pattern of clay

The XRD analysis conducted to determine the crystal structure of the clay sample revealed a significant alignment with the standard quartz pattern. Particularly, the intensity of the (011) orientations exhibited a maximum level of conformity, as depicted in Figure 2, along with other significant orientations. Quartz is abundantly present in all minerals found in nature, and it is expected that a clay, being a member of the aluminum silicate group, would demonstrate alignment in its XRD diffraction pattern with quartz. Average crystallite size (D) of clay was calculated by using Debye-Scherrer's equation (1):

$$D = \frac{k\lambda}{\beta \cos\theta} \quad (1)$$

where k is a constant (k = 0.94), λ_{Cu} is the X-ray wavelength for copper (0.15406 nm), β represents the full-width at half-maximum of the peak corrected for instrumental broadening in radians, and θ is the peak angle [8, 9]. The calculation of the average crystallite size was based on the XRD pattern's plane (011), which exhibited the highest intensity. Consequently, the average crystallite size was determined to be 57.902 nm.

3.2 FT-IR Analysis

What reveals the unique characteristics of clay is the presence of ions such as Mg, K, Ca, Fe in different proportions and, of course, its molecular structure. It was aimed to determine the functional groups in the structure of the existing organic compounds by performing FTIR characterization of the natural clay sample. The presence of illite, calcite, kaolinite and tridymite was observed in the transmittance spectrum obtained based on the mid-wavelength infrared (MIR; 400~4000 cm⁻¹) region.[13]

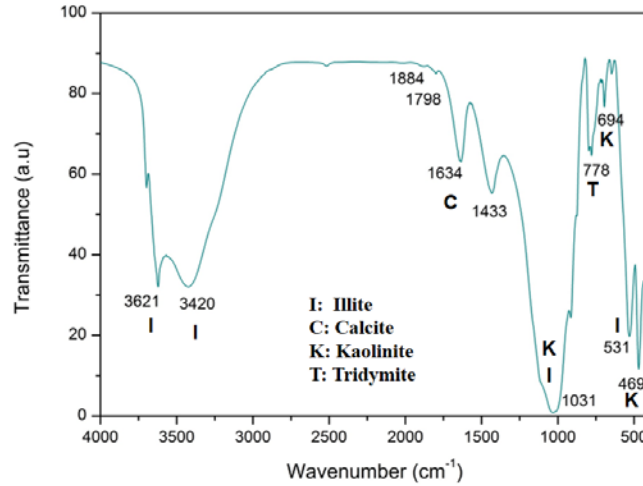


Figure 3. FTIR spectrum of clay

In accordance with the literature, the peaks marked with Si-O, O-H interactions in the structure of the quartz-based aventurine mineral and the band assignment peaks of Al and Mg are given in Table 1.

Table 1. FT-IR transmission bands assignments of clay [14, 15]

Wavenumber (cm ⁻¹)	Probable Band Assignment
469, 531	asymmetrical bending vibrations of Si-O
694	symmetrical bending vibrations of Si-O
778	symmetrical stretching vibrations of Si-O
1031	asymmetrical stretching vibrations of Si-O due to low Al for Si substitution
1433	calcite vibration
1634	inbound molecular water to Al or Mg.
1798, 1884	combination of vibrations of the Si-O network
3420	O-H, N-H group
3621	stretching vibration of O-H

3.3 SEM-EDS and, Mapping Analysis of Clay

SEM images of the clay sample shown in Figure 4 were taken at 1000 and 5000 magnifications. Although a clear morphological shape cannot be mentioned, layered structures

generally exist and fractured structures with sharp edges are seen within these layered structures. Figure 5 shows the EDX spectrum. As a result of this analysis, silicon and aluminum were present in high amounts due to alumina silicate structure. While the presence of carbon may be expected to be present in the sample, it may also have been observed due to the carbon tape used during the SEM image acquisition. Proportionally, Fe, K, Mg, Ca and Cl peaks were observed, respectively.

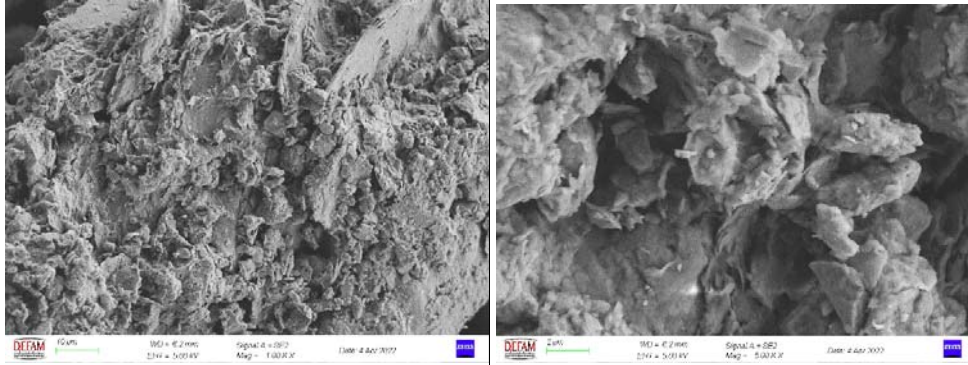


Figure 4. SEM images of clay 1000X and 5000X magnification

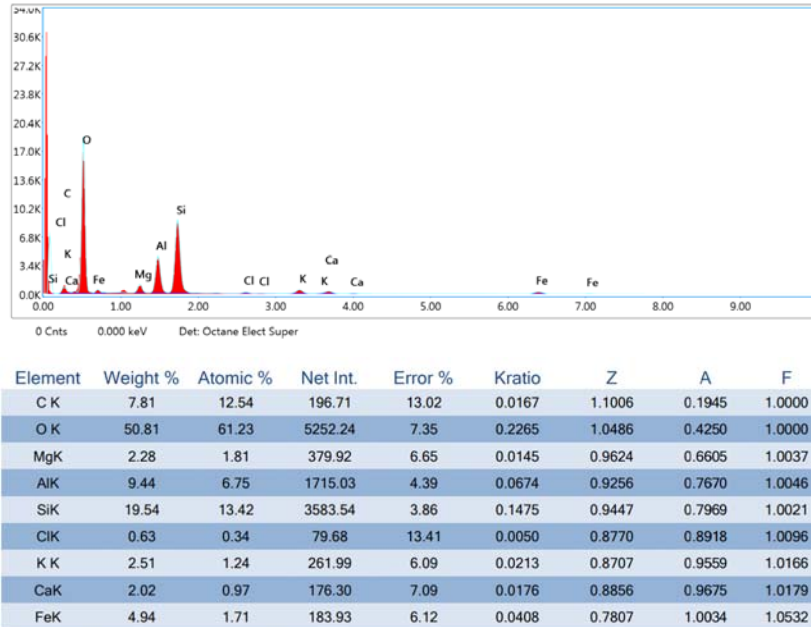


Figure 5. EDX spectrum and elemental distribution table

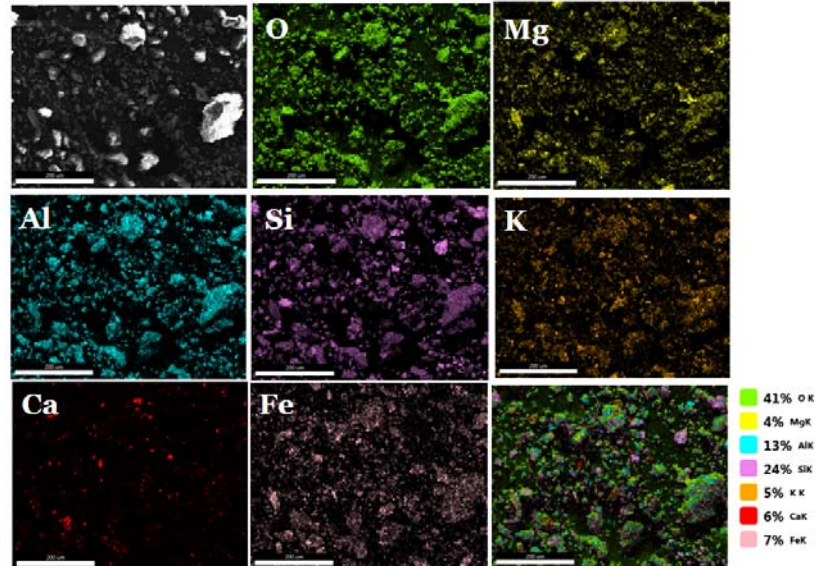


Figure 6. SEM mapping images of clay

In the mapping process in Figure 6, in addition to the presence of high amounts of silicon and aluminum, iron, calcium, potassium, and magnesium were detected in proportion, respectively.

3.4 Optical Absorption Spectrum of Clay

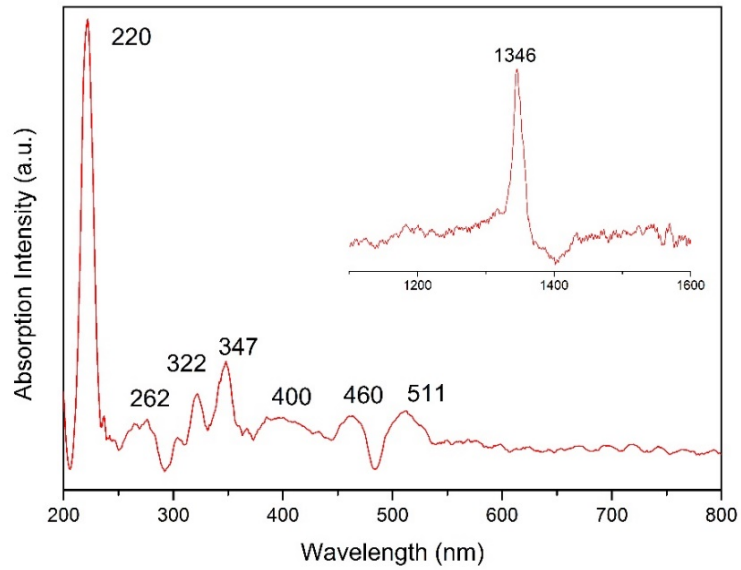


Figure 7. Optical absorption spectrum of clay

When looking at the optical absorption graph (Fig. 7), it was seen that there were absorption bands belonging to the ions contained in the clay. When evaluated in terms of the energies they absorbed; Mg^{3+} peaks were observed at 220 nm, Ca^{2+} at 262 nm and 400 nm, Fe^{3+} at 322 nm, Al^{2+} at 347 nm, Si^{4+} at 460 nm, and Mg^{1+} at 511 nm. It is thought that the peak at 1346 nm, which also appears as a sharp peak in the 1200-1600 nm range given in the graph, may be caused by Al^{1+} or Cl^{1+} ions.

3.5 Radioluminescence (RL) Spectrum

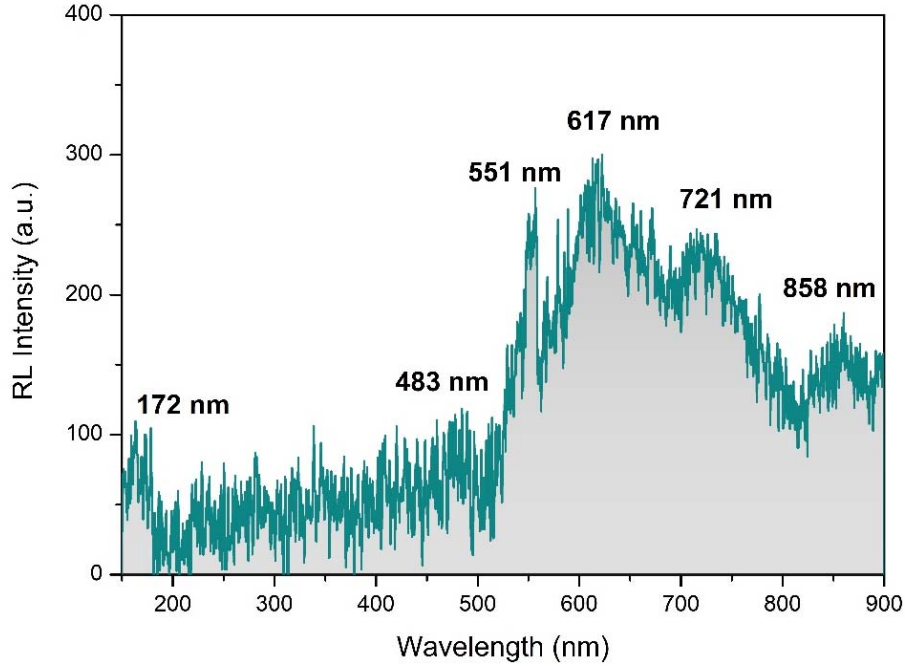


Figure 8 RL spectrum of clay

Natural clay has a relatively broad RL emission range from about 520 to 820 nm. Its shown in Figure 8 the emission bands of with maximum peak intensities at approximately 172, 483, 551, 617, 721, 870, and 858 nm.

In Table 2, transition wavelengths of silicon, magnesium, iron and aluminum at different valences are given, depending on the maximum values given in the RL spectrum. Impurities in clay, which has a very complex chemical structure, can exhibit emission due to a single transition, or they can exhibit RL spectrum as a combination of the emission bands of different ions transitioning at close wavelengths. For example, the RL band seen around 858 nm may be the combination of the emission bands of Si^{1+} , Al^{1+} and Al^{2+} valence ions, according to Table 2. RL spectrum deconvolution analysis was performed in Figure 9. Energy levels corresponding to wavelengths are shown. In addition, the CIE diagram given next to this graph shows the point where the RL spectrum of clay in the visible region coincides on the color scale[16, 17]. It can be understood that clay exposed to X-ray emits an orange, close to red, emission.

Table 2 The most intense spectral lines arranged according to wavelength [18]

Cations	Si ¹⁺	Si ²⁺	Si ³⁺	Mg ¹⁺	Mg ²⁺	Fe ¹⁺	Fe ²⁺	Fe ³⁺	Al ¹⁺	Al ²⁺	Al ³⁺
Wavelength (nm)	742	637	455	880	789	868	645	437	396	466	360
	728	566	386	518	448	649	624	592	877	600	414
	703	505	573	552	439	751	730	416	783	559	452
	594	413	482	382	-	718	542	428	669	835	569
	625	333	348	-	-	667	-	360	-	342	-
	855	784	761	-	-	-	-	-	-	-	-

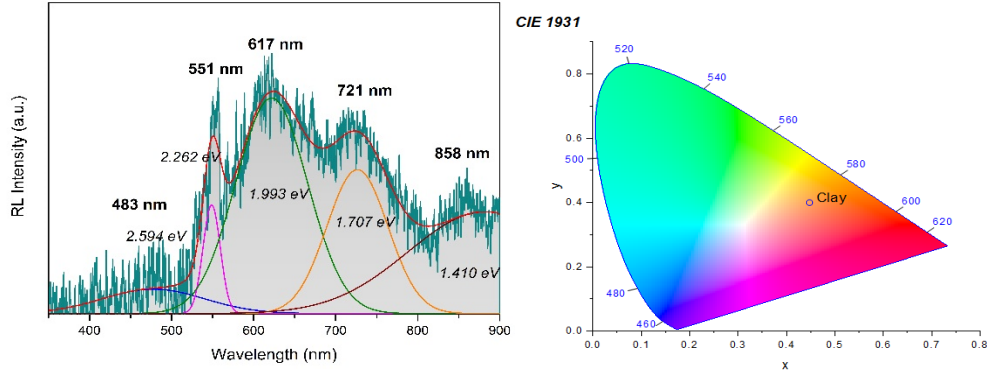


Figure 1 Fitted RL spectrum of clay and CIE diagram obtained from RL emission

3.6 Thermoluminescence (TL) Glow Curve

All minerals possess distinct characteristics such as color, luster, hardness, crystal structure, and optical properties, making them the focal point of extensive physical research. Minerals exhibit luminescence when exposed to X-rays, ultraviolet rays, cathode rays, or similar forms of ionizing radiation. The crystals constituting minerals retain energy within their structures in response to the radiation originating from their environment. This energy storage occurs as free electrons are captured by defects known as traps, which arise for various reasons in the crystal structure. [6, 7] Over time, the accumulated energy persists within the crystal structure. Thermoluminescence (TL) primarily involves the release of the stored energy in the substance by liberating the electron traps within the crystal through the controlled heating of the sample to a specific temperature.[19] The luminescence signal emitted during evacuation of the electron traps is recorded as a function of temperature.

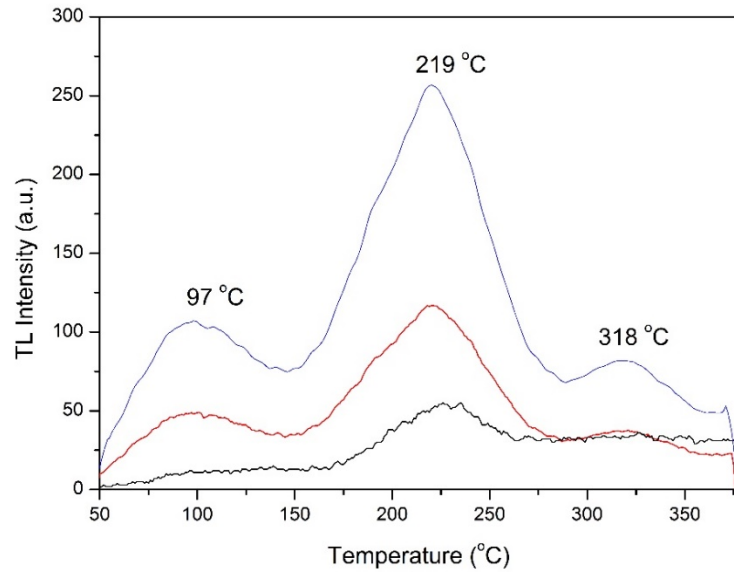


Figure 10 TL glow curves of clay after distinct X-ray exposing times

The purpose of this part of the study is to investigate the effects of radiation dose on TL glow curves. Dose response is a specific experiment performed in dosimetric studies to obtain information about the relationship between TL density and applied dose. TL spectra of natural clay were also examined by keeping the heating rate constant and changing the irradiation time (Figure 10). For this purpose, TL spectra of samples exposed to X-ray for 1 min, 5 min, 10 min were taken with a constant heating rate (2 °C/s). When the spectra were examined, it was seen that the intensity of the TL peaks obtained increased as the irradiation time increased for all heating rates. When looked at according to the periods in question, it can be seen that there is no significant change in the positions of the maximum points of the existing peaks.

The presence of glow curves at temperatures of 200°C and above, which is generally caused by deep traps, is a desirable condition in samples analyzed by TL. So much so that more electrons accumulate in these deep traps after radiation exposure and are considered to be a suitable sample for dosimetric research. However, with the presence of glow curves in deep traps, intensity is an important factor. Although the maximum intensity observed for the clay sample is not at the expected level, it has a very good intensity compared to many phosphorus samples.

4. RESULTS AND DISCUSSION

In the study, it was observed that the natural clay sample taken from Erikli Beach of Saros Gulf was highly similar to the quartz structure in the XRD analysis. FT-IR analysis showed the presence of illite, calcite, kaolinite and tridymite structures and the presence of silicon oxygen vibrations. In EDX analysis, the samples whose SEM images were taken were found to contain high amounts of iron, apart from their silicate aluminate structures. This was also supported by the mapping method. In optical absorption analysis, it was seen that the absorption bands could be attributed to metal ions in the clay. It has been stated that the natural clay sample whose RL spectrum was taken generally has emissions in the red region and that these emissions originate

from ions of different valences of silicon, aluminum, iron and magnesium. It was observed that the clay for which TL was measured had a significant glow curve around 220°C. Thus, both structural and optical characterization of the existing clay sample was carried out in the study. In subsequent studies, thermoluminescence analyzes can be expanded and kinetic parameter calculations and fading studies can also be performed.

REFERENCES

- [1] Sam Boggs, S.B.J., *Principles Of Sedimentology And Stratigraphy*, Pearson Prentice Hall.
- [2] Division, C., et al., Nanoclays For Polymer Nanocomposites , Paints , Inks , Greases And Cosmetics Formulations , Drug Delivery Vehicle And Waste Water Treatment, *29* (2006), 2, pp. 133-145
- [3] Faıza Bergaya, B. K. G. Theng, G.L., *Handbook Of Clay Science*, Elsevier Ltd, 2006
- [4] Dubey, V., et al., Thermoluminescence Study, Including The Effect Of Heating Rate, And Chemical Characterization Of Amarnath Stone Collected From Amarnath Holy Cave, *Res. Chem. Intermed.*, *40* (2014), 2, pp. 531-536
- [5] Yüksel, M., et al., Thermoluminescence Properties Of Annealed Natural Quartz After Beta Irradiation, *Luminescence*, *31* (2016), 8, pp. 1513-1518
- [6] Jose, M.T., et al., Determination Of Thermoluminescence Kinetic Parameters Of Thulium Doped Lithium Calcium Borate, *Radiat. Meas.*, *46* (2011), 10, pp. 1026-1032
- [7] da Silva, R.S., et al., Thermoluminescence Kinetic Parameters Of Bi₄Ge₃O₁₂ Single Crystals, *Nucl. Instruments Methods Phys. Res. Sect. B Beam Interact. with Mater. Atoms*, *250* (2006), 1-2, pp. 390-395
- [8] Arslanlar Tuncer Y., Kibar R., Çetin A., Canımoğlu A., A.T.Y., Radioluminescence Properties Of Copper- And Terbium-Implanted Strontium Titanate Radioluminescence Properties Of Copper- And Terbium-Implanted Strontium Titanate, *Lett. Spectrosc.*, (2013), July, pp. 364-366
- [9] Rodríguez-Lazcano, Y., et al., Thermo- And Cathodoluminescence Properties Of Lepidolite, *Spectrochim. Acta Part A Mol. Biomol. Spectrosc.*, *113* (2013), pp. 281-285
- [10] İlhan, M., et al., NIR Photoluminescence And Radioluminescence Characteristics Of Nd³⁺ Doped BaTa₂O₆ Phosphor, *Int. J. Appl. Ceram. Technol.*, *15* (2018), 6, pp. 1594-1601
- [11] Keskin, İ.Ç., İlhan, M., Thermoluminescence Kinetic Parameters And Radioluminescence Of RE³⁺ (RE = Pr, Sm, Tb, Ho, Er)-Doped Barium Tantalate Phosphors, *J. Electron. Mater.*, *52* (2023), 8, pp. 5614-5630
- [12] Keskin, İ.Ç., et al., X-Ray Irradiated Thermo- And Radioluminescence, Structural And Thermal Characterization Of Septarian (Powder&Bulk) From Madagascar, *Opt. Mater. (Amst.)*, *83* (2018), pp. 176-181
- [13] Jozanikohan, G., Nosrati, M., The Fourier Transform Infrared Spectroscopy (FTIR) Analysis For The Clay Mineralogy Studies In A Clastic Reservoir, *J. Pet. Explor. Prod. Technol.*, *12* (2022), 8, pp. 2093-2106
- [14] Ullah, R., et al., Synthesis And Characterization Of Silica Coated Iron-Oxide Composites Of Different Ratios, *Int. J. Compos. Mater.*, *4* (2014), 2, pp. 135-145
- [15] Ramasamy, V., et al., Depth Wise Analysis Of Recently Excavated Vellar River Sediments Through FTIR And XRD Studies, *Indian J. Phys.*, *83* (2009), 9, pp. 1295-1308
- [16] Keskin, İ.Ç., Radioluminescence Results, Thermoluminescence Analysis And Kinetic Parameters Of Y₂O₃:Ln³⁺ (Ln: Dy, Nd, Sm) Nanophosphors Obtained By Sol-Gel Method, *Ceram. Int.*, *48* (2022), 14, pp. 20579-20590
- [17] Keskin, İ.Ç., et al., Detailed Luminescence (RL, PL, CL, TL) Behaviors Of Tb³⁺ And Dy³⁺ Doped LiMgPO₄ Synthesized By Sol-Gel Method, *J. Lumin.*, *225* (2020), pp. 117276
- [18] Striganov, A.R., Sventitskii, N.S., *Tables Of Spectral Lines Of Neutral And Ionized Atoms*, Springer US, Boston, MA, 1968
- [19] Bayraktar, N.Ş., Krizopnas ve Rodonit ' in Termolüminesans, MSc Thesis, Erzincan Üniversitesi Fen, 2010